Control-Data Separation Architecture for Dual-Band mmWave Networks: A New Dimension to Spectrum Management

Rafay Iqbal Ansari *Graduate Student Member, IEEE,* Haris Pervaiz *Member, IEEE*, Chrysostomos Chrysostomou *Member, IEEE*, Syed Ali Hassan *Senior Member, IEEE*, Aamir Mahmood *Member, IEEE* and Mikael Gidlund *Senior Member, IEEE*

***Abstract*—The exponential growth in global mobile data traffic, especially with regards to the massive deployment of devices envisioned for fifth generation (5G) mobile networks, has given impetus to exploring new spectrum opportunities to support the new traffic demands. The millimeter wave (mmWave) frequency band is considered as a potential candidate for alleviating the spectrum scarcity. Moreover, the concept of multi-tier networks has gained popularity, especially for dense network environments. In this article, we deviate from the conventional multi-tier networks and employ the concept of control-data separation architecture (CDSA), which comprises of a control base station (CBS) overlaying the data base station (DBS). We assume that the CBS operates on the sub-6 GHz single band, while the DBS possesses a dual-band mmWave capability, i.e., 26 GHz unlicensed band and 60 GHz licensed band. We formulate a multi-objective optimization (MOO) problem, which jointly optimizes conflicting objectives: the spectral efficiency (SE) and the energy efficiency (EE). The unique aspect of this work includes the analysis of a joint radio resource allocation algorithm based on Lagrangian Dual Decomposition (LDD) and we compare the proposed algorithm with the maximal-rate (maxRx), dynamic sub-carrier allocation (DSA) and joint power and rate adaptation (JPRA) algorithms to show the performance gains achieved by the proposed algorithm.**

***Index Terms*—Control-data separation architecture, resource allocation, dual-band millimeter wave, energy efficiency, spectral efficiency, multi-objective optimization**

I. Introduction and Motivation

Fourth generation (4G) communication technology was introduced to provide a platform for supporting new services that required higher data rates. However, in order to keep pace with the rising demands of data rates and reliable communication, a need for a new generation of communication technology gained ground. According to recent estimates, the use of mobile broadband is expected to rise sharply in the coming years. The global mobile data traffic forecast report by CISCO [1] reveals that almost half a billion mobile devices were added in 2016, mainly due to the increase in the usage of smart phones. Moreover, the monthly global mobile data traffic is expected to rise to 49 exabytes by the year 2021. Viewing the massive traffic requirements of the future, the concept of fifth generation (5G) communication technology has been proposed. The major aspects of 5G network evolution include exploring new spectrum opportunities and moving towards green communication.

Heterogeneous network (HetNet) is one of the key enabling technologies of 5G networks. HetNets allow base station (BS) densification by allowing a multi-tier network with macrocells overlaid with small cells (micro, pico and femto). The small cell BSs (SBSs) are low-power radio access nodes with a limited range [2]. HetNets, by allowing spatial reuse of spectrum resources, lead to higher network capacity. The main objective of introducing the small cells is to ease the load on the macrocells by offloading traffic to small cells. The short distance between the transmitter and receiver in small cells enhances radio link quality, which in turn leads to higher data rates. In addition to this, the (30 GHz to 300 GHz) millimeter wave (mmWave) frequency band is considered as a viable candidate for meeting the new service demands and overcoming the spectrum congestion. The mmWave frequency band promises higher bandwidth, providing a much needed space for offloading traffic from the licensed bands.

The channel propagation conditions in mmWave frequency bands necessitate directional beamforming, which leads to low interference [3]. The beamforming techniques are further classified into analog, digital and hybrid beamforming, where the choice of a particular beamforming technique depends on the processing and power consumption constraints [4]. Moreover, the high frequency of mmWave bands allows small antenna dimensions, which could help in miniaturization of devices. The mmWave technology, however, has some limitations that include low transmission range and high penetration loss due to obstacles, which requires establishing line-of-sight (LoS) transmission links. Integration of mmWave small cells with the traditional long term evolution (LTE) based macrocells can lead to numerous new opportunities for services requiring higher data rates. However, to maximize gain of such integration, efficient resource allocation, user association and power management techniques are required to ensure energy efficiency (EE) as well as spectral efficiency

R. I. Ansari and C. Chrysostomou **(Corresponding Author)** are with the Department of Computer Science and Engineering, Frederick University, Nicosia, Cyprus. Emails: rafay.ansari@stud.frederick.ac.cy, ch.chrysostomou@frederick.ac.cy.

H. Pervaiz is with School of Computing and Communications, Lancaster University, UK. Email: h.b.pervaiz@lancaster.ac.uk.

S. A. Hassan is with the School of Electrical Engineering & Computer Science (SEECS), National University of Sciences and Technology (NUST), Pakistan. E-mail: ali.hassan@seecs.edu.pk.

A. Mahmood and M. Gidlund are with Department of Information Systems and Technology, Mid Sweden University, 851 70 Sundsvall, Sweden. Emails: {aamir.mahmood, mikael.gidlund}@miun.se.

(SE). Recently, control-data separation architecture (CDSA) [5] has been proposed as one of the solutions to cater to the limitations of conventional HetNets. The main concept behind CDSA is to separate the control plane (CP) and the data plane (DP), providing ubiquitous connectivity in dense networks. The CDSA architecture includes control BSs (CBSs) that correspond to the macrocells, while the data BSs (DBSs) correspond to the small cells, which overlay the CBSs.

In this work, we consider a radio access network (RAN) architecture with CDSA for a downlink transmission. The mmWave DBSs operate on unlicensed 26 GHz and licensed 60 GHz bands, while the CBS utilizes the 2.4 GHz band. The integration of sub-6 GHz band based CBSs with mmWave empowered DBSs can provide significant performance gains. High range of 2.4 GHz band allows the CBS to conduct signaling activities and provide connectivity to users, which fall outside the transmission range of DBSs. The DBSs with low range provide high data rates to the users, which fall within their transmission range, while causing negligible interference due to low range and transmissions with high directivity. To the best of our knowledge, no prior study has been performed that considers a EE-SE tradeoff analysis for the dual-band mmWave network based on CDSA.

The key contributions of this work are summarized as follows.

- Different from the conventional EE and SE optimization approaches, we formulate a multi-objective optimization (MOO) problem, which jointly optimizes conflicting objectives to analyze the SE and EE tradeoff in a CDSA-based network environment. The MOO problem is transformed into a tractable single objective problem by using the weighted Tchebycheff method.
- We develop a joint radio resource allocation algorithm based on Lagrangian Dual Decomposition (LDD). The LDD-based algorithm jointly optimizes the decisions with regards to power allocation for CBS, DBSs and sub-carrier pair allocation. We compare the performance of the network involving single-band and dual-band mmWave DBS.
- We compare the performance of the proposed LDD-based algorithm with the maximal-rate (maxRx), dynamic sub-carrier allocation (DSA) and joint power and rate adaptation (JPRA) algorithms in terms of SE and EE, thereby highlighting the gains achieved through dynamic spectrum management in the presence of licensed and unlicensed mmWave resources. The results reveal that the LDD-based algorithm outperforms the aforementioned algorithms in terms of EE and SE.

The rest of the paper is organized as follows. In Section II, we discuss the related work and briefly describe the advantages and limitations of CDSA. In Section III, we discuss the system model by explaining the initial radio access design, followed by the channel model and the network rate formulation. The optimization problem formulation for resource allocation is presented in Section IV. Section V presents the simulation model and results, and Section VI outlines the conclusions.

II. Related Work: Resource Allocation Tehchniques and CDSA

In this section, we first present a review of the resource allocation techniques in multi-tier networks. Next, we discuss both the advantages and disadvantages provided by CDSA.

A. Resource Allocation Techniques

Several studies have focused on devising a resource allocation scheme for multi-tier networks. Authors in [6] present a hierarchical game-theoretic approach for optimal resource allocation in HetNets. The authors propose a network-assisted user-centric access design and the performance analysis reveals enhanced performance of the proposed technique as compared to the network-centric access scheme. In [7], a downlink HetNet environment is considered and a user association strategy is presented, where the users can associate with multiple BSs. A BS transmit power optimization problem is also presented where BSs possess the flexibility of varying their transmit power and turn themselves off at low-peak times. Similarly, [8] discusses the challenge of high energy consumption in network scenarios involving dense deployment of SBSs. The authors propose an energy efficient user association and SBS on/off switching scheme to minimize the total power consumption. The number of active SBSs varies according to the network requirement to reduce the power consumption.

The prior work on resource allocation in HetNets has mainly focused on a single band links based on sub-6 GHz microwave links. Recently, the concept of dual-band for HetNets has been explored, which envisions a combination of microwave and mmWave frequency bands. The dual-band approach allows to exploit the benefits from propagation characteristics of both frequency bands [9]. One of the major advantages of this approach is the interference avoidance between LTE based macrocell and mmWave small cells. Moreover, the low range of mmWave small cells provides the opportunity for isolated transmission, which leads to negligible intra-cell interference. A dual-band framework for multi-hop relay network was introduced in [10], where the HetNet model is based on mmWave and LTE bands to meet the desired quality-of-service (QoS) at the users. The downlink resource allocation problem for HetNet is presented as an optimization problem, where the results highlight the enhanced performance of dual-band strategy in terms of achievable rate. Authors in [11] discuss a joint user association and power allocation optimization problem for mmWave-based ultra dense network with energy harvesting BSs. The optimization design is based on QoS constraints, energy efficiency, limits on cross-tier interference and energy harvesting by BSs. The proposed scheme also considers an interference coordination mechanism to limit the interference between BSs and users. A heuristic quality-of-experience (QoE) based user association problem is presented in [12], where the profit of mobile network operators is maximized while ensuring the QoE experienced by the user. In this study, the macrocell base station (MBS) works on microwave band while the SBS works on the mmWave frequency band. A comparison between proposed scheme and signal-to-interference plus noise ratio (SINR)-based algorithm

is presented and the performance gains in terms of QoE and higher profit are quantified through simulation results.

Energy aware system design is important in future 5G networks, which aligns with the vision of green communication technologies. Several works have appeared in literature, which focus on ensuring the EE in HetNets [13]–[16]. All the aforementioned works focus on maximizing the EE only. However, some works have followed another approach of jointly analyzing the SE-EE tradeoff [17]–[19]. The SE-EE tradeoff analysis is significant for designing energy efficient communication system. Authors in [17] present an optimization problem for maximizing the EE and SE for HetNet coordinated multi point (CoMP) for orthogonal frequency-division multiple access (OFDMA) networks. The network environment considered includes a MBS underlaid by several low-power radio resource heads (RRH) based on 2.6 GHz band. The power consumption model also includes the transmit power required for fiber backhauling. In [18] and [19], a multi-tier HetNet is considered and the authors present a green cell assocation (GCA) scheme, where the energy efficiency is based on a metric defined as spectrum efficiency per unit power consumption. The performance of GCA scheme is compared to the maximum received power association (MRPA) and nearest BS association (NBA) schemes, where GCA scheme outperforms the other schemes in terms of EE. Authors in [20] present a EE and SE tradeoff analysis for uplink of multi-user two-tier OFDMA HetNet subject to users' maximum transmit power and minimum rate constraints. Authors in [21] discuss a dense multi-tier HetNet with LoS and NLoS transmissions. The downlink coverage probability is derived, which helps in determining the area spectral efficiency (ASE) and EE of the network. The authors observe that in the case of highly dense SBS deployment, increase in the transmit power of SBS does not improve the ASE but decreases the EE. Moreover, it is also observed that in dense HetNets, the ASE and EE increases with an increase in SBS density due to the dominance of LoS links. Considering the spectrum constraints in the future dense HetNets, it is important that the network optimization and analysis address both SE and EE to give a more realistic picture of the network performance.

Recently, some works have appeared in literature exploring the possibilities of a dual-band transmission mechanism. In [22], authors present the idea of new transceivers that allow hybrid mmWave based HetNet, i.e., dual bands to operate at the SBS. The utilization of dual-band allows reduction in interference and allows the choice of transmission in a particular band depending on the propagation characteristics and the QoS requirements. Authors in [23] present a dual-band antenna design specifically designed for operation at 25 GHz and 37 GHz mmWave bands. These works highlight the need to overcome the hardware constraints for dual-band network operation. The performance analysis of dual-band network operation has also been conducted in the literature, providing an idea about the performance gains that can be achieved. Authors in [10] utilize the concept of dual-band to optimize the normalized sum-weighted rate of the system. The mmWave bands considered for operation are the 60 GHz V-band and the 70-80 GHz E-band. The results signify the importance of using multiple-band approach for HetNets. In [24], the authors carry the concept of dual-band transmission further by proposing a new architecture for multi-band multiple-input multiple-output (MIMO) HetNet. Two deployment scenarios are considered: a) MBS works on the microwave and mmWave band while the SBS works on the mmWave band, and b) the dual-band capability is reversed and the MBS works on single microwave band while the SBS works on dual-band. The approximate distance of the user from the BS is considered for selecting a particular band of operation, e.g., if the user is at a distance greater than a particular threshold microwave link is selected, otherwise mmWave link is selected for transmission. The results highlight the performance gains achieved through applying the dual-band approach at the small cells.

In this work, we build on the platform provided by the aforementioned works to develop and analyze a resource allocation problem for dual-band mmWave network environment based on CDSA.

B. Control-Data Separation Architecture

The main objective of CDSA is to separate the signals for full coverage from high data rate transmissions. The CP usually operates on low frequency bands with good propagation capabilities to provide high coverage. The DP can operate on high frequency bands, offering high capacity and more spectrum resources. Initially, the users are not connected to DBS and the idle users are connected to CBS only. The CBS can initiate a call or a data session for the user by finding the suitable DBS to provide high data rates. CDSA approach can lead to energy saving by avoiding the always *on* paradigm. CDSA provides a re-configurable approach to adapt to the changes in the network, allowing a scalable solution through load dependent deployment of DBSs. The CDSA can dynamically adapt to the traffic loads to provide considerable energy savings by switching the DBS *on/off* according to the predicted/measured average traffic loads based on the historical information. It is pertinent to note that switching *off* a DBS doesn't lead to loss of coverage for the devices as the CBS provides ubiquitous connectivity to the devices. The DBS can be activated by the CBS, if the device moves within the coverage range of an inactive DBS, well in advance based on the device's mobility pattern in order to be active before the device arrival to provide the data transmission. If a user moves from the coverage area of one DBS to another, the CBS helps in associating the user with the best serving DBS. The separation of control and data plane allows the CBS to carry out dynamic readjustments to the network through ubiquitous control signaling, while the operation of DBS is limited to the data plane.

Despite the benefits of CDSA over traditional RAN architecture, there are also several challenges. The CBS requires channel information of each DBS-user link, which could lead to significant overhead. One method to determine channel information is through gathering the position information of devices through the global positioning system (GPS) [5]. The channel prediction models could help in determining the channel state of DBS-device links. Furthermore, a backhaul connection is required to support the coordination between CBS

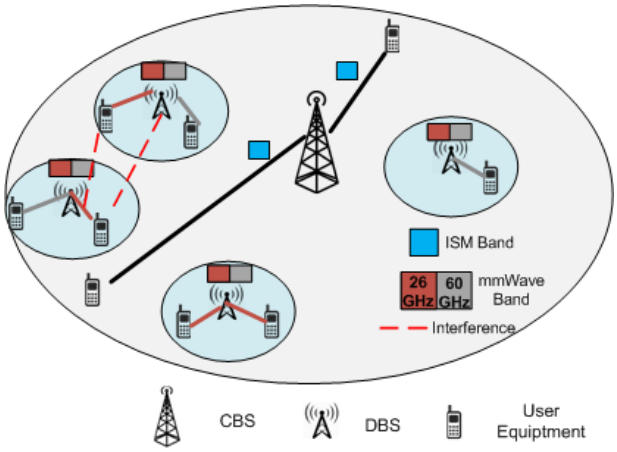

Fig. 1: Snapshot of a typical CDSA-based network with CBS overlaying dual-band DBSs. CBS operates at 2.4 GHz ISM band, DBS operates at 26 and 60 GHz mmWave bands.

TABLE I: Notations

$\mathcal{B}_M$	{1...M} Set of CBSs $m \in \{1, 2, ..M\}$
$\mathcal{B}_L$	{1...L} Set of DBSs $l \in \{1, 2, ..L\}$
$\mathcal{U}_m$	Set of all users randomly deployed in the coverage area of CBS m, $u \in \mathcal{U}_m$
$\mathcal{F}$	Set of frequency bands, $\mathcal{F} \in \{f_1, f_2, f_3\}$ 2.4 GHz, 26 GHz and 60 GHz, respectively
$\mathcal{N}$	Set of orthogonal subcarriers, $n \in \mathcal{N}$, $\mathcal{N} = N_1, N_2, N_3$
w_u	Weight of user u according to required QoS
$\rho^{(n)}_{m,u}$	Binary operator showing allocation of subcarrier n to user u for CBS m
$\rho^{(n)}_{l,u}$	Binary operator showing allocation of subcarrier n to user u for DBS l
T	Time required for beamforming, user association and data transfer
θ_l	DBS beamwidth
θ_u	User beamwidth

and DBSs leading to a high system overhead. The solution to the high overhead lies in designing new signaling techniques for CBS and DBS. The dual connectivity of devices to CBS and DBS requires an uplink-downlink decoupling along with the logically separated CP and DP. It is important to note that the optimal DBS-user link for an uplink transmission scheme might be different from the downlink transmission scheme, which implies that different resource allocation schemes will be required for uplink and downlink transmission, respectively.

III. System Model

We consider a network, where multiple DBSs are overlaid within the coverage area of a CBS, as shown in Fig. 1. In this network, there are U_m users randomly distributed within the coverage area of CBS, denoted as $\mathcal{U}_m = \{1, 2, \cdots, U_m\}$ and the set of BSs or access points (APs) as $\mathcal{B} = \{\underbrace{1, 2, \cdots, M}_{\mathcal{B}_M}, \underbrace{M+1, \cdots, M+L}_{\mathcal{B}_L}\}$, where $\mathcal{B}$ represents the total number of APs such that there are M CBSs operating at $f_1 = 2.4$ GHz industrial, scientific and medical (ISM) band and L DBSs within each CBS, where L is the number of DBSs operating at $f_2 = 26$ GHz and $f_3 = 60$ GHz, such that $\mathcal{B} = \mathcal{B}_M \cup \mathcal{B}_L$. The number of subcarriers at each frequency band f_1, f_2 and f_3 are denoted by N_1, N_2 and N_3, respectively. The notations used throughout this paper are outlined in Table I. The CDSA approach can be further classified into two cases:

- *Case 1*: The CBS supports the CP only, while the DBS supports the DP.
- *Case 2*: The CBS supports the CP as well as DP, while the DBS supports the DP.

In this work, we focus on Case 2 from the radio resource management perspective. The CBS transmits directly to the user by using 2.4 GHz band. The DBSs are assumed to posess the capability to operate at 26 and 60 GHz bands. We assume time division duplexing (TDD) scheme, allowing the BS to estimate channel parameters due to channel reciprocity. We start by first defining the initial access model and determining the beamforming gains observed at different modes of operation. Next, the normalized end-to-end achievable rate and power consumption model are presented.

A. Antenna Characteristics and the Initial Access

The transmitter and receiver undergo a beam training procedure to gain maximum benefit from the antenna gain in the main lobe and establish the best mmWave link. In the first step, the transmitter and receiver identify the sector level beams by using pilot transmissions. In the next step, the optimal beams are identified from within the selected sector. Narrow beams could lead to higher antenna gains, but at the cost of higher beam training overhead [25]. In this work, we assume that sector level beam alignment has already been established as part of routing [26]. The sector level beamwidths are given as φ_l and φ_u for DBS and user, respectively. The time required for pilot transmission is denoted by T_p. Neglecting the sector level alignment, the duration of alignment procedure is given as

$$\tau_{u,l} = \left\lceil \frac{\varphi_l}{\theta_l} \right\rceil \left\lceil \frac{\varphi_u}{\theta_u} \right\rceil T_p \text{ for DBS}, \tag{1}$$

where $\lceil . \rceil$ represents the ceiling function which returns the smallest following integer and θ_l and θ_u denote the beam-level beamwidths of DBS and user, respectively. The beamforming gain at a user u is given by [27]

$$G(\theta_u) = \begin{cases} \frac{2\pi}{\theta_u}\left(\frac{\gamma}{\gamma+1}\right) & \text{main lobe}, \\ \frac{2\pi}{2\pi-\theta_u}\left(\frac{1}{\gamma+1}\right) & \text{side lobe}, \end{cases} \tag{2}$$

where γ models the front-back ratio, i.e., $\gamma = \frac{2\pi}{C_o(2\pi-\theta_u)}$, C_o is a constant that is taken as 10 dB [27]. The completion of the beamforming phase marks the start of the data transmission phase. The alignment period $\tau_{u,l}$ should be less than T, where T is the total time slot duration. Although lower beamwidth could provide high directivity, there is a physical constraint to the minimum value of beamwidth depending on the antenna configuration. In this work, we assume that the antenna patterns are approximated by the sectorized beam pattern, where constant main lobe gain is observed. For the DBS, we assume a high front-to-back ratio, γ, and zero side lobe gain, whereas the main lobe gain is $G(\theta_l) = \frac{2\pi}{\theta_l}$.

B. Problem Formulation

In the proposed model, the user has the option to associate with any AP from CBS or DBSs, depending on the QoS criteria. The rate formulation involves the analytical expressions for the downlink transmission through all the APs. To characterize the rate observed at the user, we define the received SINR of the u^{th} user served directly by CBS $m \in B_M$ at the n^{th} subcarrier as

$$\Gamma^{f}_{m,u} = \frac{h_{m,u,n} G(\theta_u) P_{m,u,n} \left(\frac{\lambda_f}{4\pi}\right)^2 d^{-\alpha_f}_{u,m}}{N_0 + I_{u,n}}, \quad f \in \mathcal{F}, \tag{3}$$

where $P_{m,u,n}$ is the power allocated for the u^{th} user on the n^{th} subcarrier of the m^{th} CBS and is given by $P_{m,u,n} \in (0, P^{\max}_m]$ for the case when the user occupies the n^{th} subcarrier of the m^{th} CBS and otherwise it is zero, $I_{u,n}$ is the total interference at the u^{th} user on the n^{th} subcarrier from the other CBSs operating at the 2.4 GHz band, N_0 is the noise power, λ_f is the wavelength of 2.4 GHz band, α_f is the pathloss exponent of 2.4 GHz band, $d_{u,m}$ is the distance between the m^{th} CBS and the u^{th} user, and $h_{m,u,n}$ is the channel gain.

The mmWave signals undergo penetration losses to physical structures such as buildings. For example, the authors in [28] present the penetration loss measurements for indoor environments due to different materials such as glass doors, walls and steel. The impact of antenna polarization at the transmitter and the receiver is also quantified. For example, the average penetration loss incurred by the walls when both the transmitter and the receiver antennas are vertically polarized is 10.6 dB, while the penetration loss in case where transmitter antenna is vertically polarised and receiver antenna is horizontally polarized is found to be 11.7 dB. The severe penetration loss due to obstacles is one of the limiting factors observed in the mmWave based transmission links and leads to different LoS and NLoS path loss characteristics. Highly directional communications are used for mmWave links to avoid the penetration losses. In this work, we consider both LoS and NLoS links by modeling the blockages as a rectangular Boolean scheme as in [29]. The LoS probability function is denoted by $\mathbb{P}(d)$ and is defined as

$$\mathbb{P}(d) = e^{-yd}, \tag{4}$$

where d is the distance between the transmitter and the receiver, y is a parameter dependent on the distribution and size of the blockages, and $1/y$ is the average LoS range of the network. We assume Nakagami fading for mmWave links, where the path loss exponent α_f and the shadowing for LoS and NLoS differ and are denoted by parameter $\mathcal{X}^{LoS}_{mmW}$ and $\mathcal{X}^{NLoS}_{mmW}$, respectively. The SINR of users served directly by DBS over 26 GHz and 60 GHz mmWave band is given as

$$\Gamma^{f}_{l,u} = \frac{h_{l,u,n} G(\theta_u) P_{l,u,n} \left(\frac{\lambda_f}{4\pi}\right)^2 d^{-\alpha_f}_{u,l}}{N_0 + I_{u,n}}, \quad f \in \mathcal{F}, \tag{5}$$

where $P_{l,u,n}$ is the power allocated for the u^{th} user on the n^{th} subcarrier of the l^{th} DBS and is given by $P_{l,u,n} \in (0, P^{\max}_l]$ for the case when the user occupies the n^{th} subcarrier of the l^{th} DBS and otherwise it is zero, $I_{u,n}$ is the total interference at the u^{th} user on the n^{th} subcarrier from the other DBSs, N_0 is the noise power, λ_f is the wavelength of mmWave (26 GHz or 60 GHz), α_f is the pathloss exponent, $d_{u,l}$ is the distance between the l^{th} DBS and the u^{th} user, and $h_{l,u,n}$ is the channel gain.

In this work we assume that the the mmWave DBSs are deployed such that the inter-tier interference is negligible. SINR expressions in (3) and (5) are useful in defining the end-to-end rate observed at the user when served by CBS and DBS.

We proceed with defining the achievable rate of the user when served by different BSs. The normalized maximum achievable rate of the user u served by CBS m is defined as

$$\begin{aligned} C_{m,u} &= \sum_{S_m} \rho^{(n)}_{m,u} w_u \left[\log_2\left(1 + \Gamma^{f}_{m,u}\right)\right] \\ &= \sum_{S_m} \rho^{(n)}_{m,u} C^{(n)}_{m,u}, \end{aligned} \tag{6}$$

where $S_m = \{n, u, m | n \in \mathcal{N}; u \in \mathcal{U}_m; m \in \mathcal{B}_M\}$.

The achievable rate of the user u served via direct link by DBS is defined as

$$\begin{aligned} C_{l,u} &= \sum_{S_m} \left(1 - \frac{\tau_{u,l}}{T_t}\right) \rho^{(n)}_{l,u} w_u \left[\log_2(1 + \Gamma^{f}_{l,u})\right] \\ &= \sum_{S_m} C^{n}_{l,u} \end{aligned} \tag{7}$$

The beamforming overhead $\tau_{u,l}$ impacts the achievable rate at the user, where the transmissions take place only after the initial connection setup, which leave a portion of the total time slot T_t for transmission.

Now, we define the total normalized achievable rate for each user u, which is given by

$$C_u = \left\{\mu_u C_{l,u} + (1 - \mu_u) C_{m,u}\right\}, \tag{8}$$

where $\mu_u \in \{0, 1\}$ is a binary parameter, where $\mu_u = 1$ denotes direct transmission through DBS and $\mu_u = 0$ denotes direct transmission through CBS. This binary parameter defines the mode selection of the user, where we will show later that the users are associated with a particular AP based on a multi-objective optimization problem. The normalized system throughput over bandwidth is then defined as

$$C^{\text{total}} = \sum_{u \in \mathcal{U}_m} C_u, \tag{9}$$

which also represents the SE of the network.

C. Power Consumption Model

The total power consumption of the transmissions is denoted by P_{total}, which is equal to the sum of total circuit power, P_{C}, and the total power consumed by the network P_t. To determine the expression for P_t, we first define the total power consumed for each user $u \in \mathcal{U}_m$ as

$$P_{t_u} = \underbrace{\mu_u \sum_{S_m} \rho^{n}_{l,u} p_{tot,l}}_{P^{l}_{t}} + \underbrace{(1 - \mu_u) \sum_{S_m} \rho^{n}_{m,u} p_{tot,m}}_{P^{m}_{t}} \tag{10}$$

where $p_{tot,m} = P_{m,u,n}$ and $p_{tot,l} = P_{l,u,n}$ are the total powers consumed by CBS and DBSs, respectively. The total power consumed for transmissions is defined as

$$P_t = \sum_{u \in \mathcal{U}_m} P_{t_u}. \tag{11}$$

Now, we define the total power consumption as $P_{total} = P_c + \eta P_t$, where $1/\eta$ is the power amplifier efficiency. The circuit power P_{C} is a combination of the power consumed by phase shifters, radio frequency (RF) chains, and amplifiers [30]. The total power consumption helps in quantifying the EE of the network, which is defined as the transmitted bits per unit energy, i.e.,

$$EE = \frac{C^{total}}{P_{total}}. \tag{12}$$

IV. Resource Allocation Problem Formulation

The performance objective is to maximize two factors, the SE and the EE, which poses a problem involving two factor tradeoff.

A. Multi-objective optimization problem formulation

The resource allocation problem under minimum rate requirement for each user is given as

$$\mathbb{P}_1 \quad \max_{(\boldsymbol{\rho},\boldsymbol{p})} \quad \sum_{u \in \mathcal{U}_m} C_u \tag{13a}$$

$$\max_{(\boldsymbol{\rho},\boldsymbol{p})} \quad -P_{total} \tag{13b}$$

$$\text{s.t.} \tag{13c}$$

$$\text{C1}: \quad C_u \geq C_{\min} \quad \forall u \in \mathcal{U}_m \tag{13d}$$

$$\text{C2}: \quad P_t^m \leq P_m^{\max} \quad \forall m \in \mathcal{B}_M \tag{13e}$$

$$\text{C3}: \quad P_t^l \leq P_l^{\max} \quad \forall l \in \mathcal{B}_L \tag{13f}$$

$$\text{C4}: \quad p_{tot,\text{mode}} \geq 0 \quad \forall n, u, \text{mode} \in \{m, l\} \tag{13g}$$

$$\text{C5}: \quad \mu_u \in \{0,1\} \forall u \in \mathcal{U}_m \tag{13h}$$

$$\text{C6}: \quad \rho_{m,u}^n, \rho_{l,u}^n \in \{0,1\} \tag{13i}$$

where $\boldsymbol{p} = \{p_{tot,\text{mode}}\}$ and $\boldsymbol{\rho} = \{\rho_{\text{mode},u}^n\}$. Constraint C1 ensures that the user rate is greater than $C_{\min}$. The restriction that users should maintain a minimum data rate C_{min} is important for practical network operation. Constraint C2 signifies that the maximum transmit power of a CBS doesn't exceed a threshold. Similarly, constraint C3 is the maximum transmit power constraints for DBS. Constraint C4 ensures that total power consumed is greater than zero. Constraint C5 ensures that the user is connected with a particular mode, i.e., direct mode through CBS or DBS. Constraint C6 signifies subcarrier selection for each mode.

B. Solution of Optimization Problem

The objective function in (13) can be used to analyze the EE-SE tradeoff of the network. The multi-objective optimization problem of (13) can be transformed into single objective optimization problem by using the weighted Tchebycheff method [31] and normalizing the two objectives as

$$\mathbb{P}_2 \quad \Phi \frac{C^{tot}}{R_{norm}} - (1-\Phi)\frac{P_{total}}{P_{norm}} \tag{14a}$$

$$s.t. \quad C1 - C6 \tag{14b}$$

where $\Phi \in [0,1]$ assigns the weight to each objective, i.e., $\Phi = 0$ signifies that the objective reduces to power minimization problem, while with $\Phi = 1$ the objective reduces to rate maximization problem. As each objective has a different magnitude, we normalized them to ensure consistency in the comparison. Normalization ensures that the Pareto optimal solution is consistent with the weights assigned. As the MOO problem comprises of two conflicting objectives, the Pareto optimal solution provides the best values for these objectives.

Proposition 1. *For any weighting parameter Φ, (14) is a convex optimization problem.*

Proof. See Appendix □

Next, we relax the constraints C1-C3 to determine the LDD-based solution. We now derive the optimization solution to the multi-objective problem in $\mathbb{P}_2$ given as

$$\begin{aligned}\mathcal{L}(\boldsymbol{\rho}, \boldsymbol{p}, \boldsymbol{\lambda_u}, \boldsymbol{X_m}, \boldsymbol{Y_l}) &= \Phi \frac{C^{tot}}{R_{norm}} - (1-\Phi)\frac{P_{total}}{P_{norm}} \\ &- \sum_{u \in \mathcal{U}_m} \boldsymbol{\lambda_u}(C_{min} - C_u) - \boldsymbol{X_m}(P_t^m - P_{max}^m) \\ &- \boldsymbol{Y_l}(P_t^l - P_{max}^l)\end{aligned} \tag{15}$$

where $\boldsymbol{\lambda_u} = \{\lambda_1, \lambda_2, \lambda_u\}\ \forall u \in \mathcal{U}_m$, $\boldsymbol{X_m} = \{X_1, X_2, X_m\}\ \forall m \in M$, $\boldsymbol{Y_l} = \{Y_1, Y_2, ..Y_l\}\ \forall l \in L$ are Lagrange multiplier vectors corresponding to the constraints C1, C2 and C3, respectively. The function presented in (15) is a convex optimization problem, which means that the duality gap between primal and dual solutions is zero and solving its dual problem is the same as solving the original problem. The Lagrangian dual function for (15) is given as

$$q(\boldsymbol{\lambda_u}, \boldsymbol{X_m}, \boldsymbol{Y_l}) = \quad max \quad \mathcal{L}(\boldsymbol{\rho}, \boldsymbol{p}, \boldsymbol{\lambda_u}, \boldsymbol{X_m}, \boldsymbol{Y_l}) \tag{16a}$$

$$s.t. \qquad C4 - C6 \tag{16b}$$

The corresponding dual optimization problem is then denoted by

$$\min_{(\boldsymbol{\lambda_u} \geq 0, \boldsymbol{X_m} \geq 0, \boldsymbol{Y_l} \geq 0)} \quad q(\boldsymbol{\lambda_u}, \boldsymbol{X_m}, \boldsymbol{Y_l}) \tag{17a}$$

$$s.t. \qquad \text{C4-C6} \tag{17b}$$

We now proceed with finding the optimal power allocation by applying the Karush-Kuhn-Tucker (KKT) condition, which involves computing the derivative of the Lagrangian function defined in (16) and setting it to zero. The optimal power allocation then contributes in finding the optimal subcarrier pair allocation. Lemma 1 defines the expressions for optimal power allocation.

Lemma 1: *The optimal power allocation is given as*

$$\overline{P_{l,u,n}} = \left[m_1 - \frac{1}{H_1^n}\right]^+, \tag{18a}$$

$$\overline{P_{m,u,n}} = \left[m_2 - \frac{1}{H_2^n}\right]^+, \tag{18b}$$

where $[x]^+$ *corresponds to* $max\{0, x\}$ *and*

$$m_1 = \frac{(1 - \frac{\tau_{u,l}}{T_t})w_u H_1^n(\Phi + \lambda R_{norm})P_{norm}}{(Y_m P_{norm} + (1-\Phi)\eta)(ln(2)R_{norm})}, \tag{19a}$$

$$m_2 = \frac{w_u H_2^n(\Phi + \lambda R_{norm})P_{norm}}{(X_m P_{norm} + (1-\Phi)\eta)(ln(2)R_{norm})}, \tag{19b}$$

and $H_1^n = \frac{h_{l,u,n} G(\theta)\left(\frac{\lambda_f}{4\pi}\right)^2 d_{u,l}^{-\alpha_f}}{N_0 + I_{u,n}}$, $H_2^n = \frac{h_{m,u,n} G(\theta)\left(\frac{\lambda_f}{4\pi}\right)^2 d_{u,m}^{-\alpha_f}}{N_0 + I_{u,n}}$

Proof. See Appendix □

Now, we define $\varphi_n^{\mathcal{B}}$ as the impact factor of the link $(n, \mathcal{B})$ to $\mathcal{L}(\boldsymbol{\rho}, \boldsymbol{p}, \boldsymbol{\lambda_u}, \boldsymbol{X_m}, \boldsymbol{Y_l})$. For example, for CBS mode the impact factor is given as

$$\varphi_n^{\mathcal{B}_M} = \frac{(\Phi - \lambda_u)}{R_{\text{norm}}} - \left[\frac{(1-\Phi)\eta}{P_{\text{norm}}} + X_m\right]\overline{P_{m,u,n}}, \tag{20}$$

which can be easily found through expanding the expression given in (15) and taking common all the factors related to CBS mode. A similar process is applied to find impact factor of transmissions through DBS, which is denoted by $\varphi_n^{\mathcal{B}_L}$. The impact factor allows the fragmentation of the original Langragian function given in (15) into $(M + L + N^2)$ sub-problems which is denoted by

$$\mathcal{L}(\rho_{\text{mode},u}^n, \overline{P_{\mathcal{B},u,n}}, \lambda_u, X_m, Y_l) = \varphi_n^{\mathcal{B}} \rho_{\mathcal{B},u}^n. \tag{21}$$

To maximize $\mathcal{L}(\boldsymbol{\rho}, \boldsymbol{p}, \boldsymbol{\lambda_u}, \boldsymbol{X_m}, \boldsymbol{Y_l})$, the subcarrier n is allocated to AP-user pair with maximum achievable value of $\varphi_n^{\mathcal{B}}$.

The optimal solution to (15) can be obtained by using the sub-gradient method, where the dual variables are updated as

$$\lambda_u^{k+1} = [\lambda_u^k + \omega^k(C_{min} - C_u)]^+, u \in \mathcal{U}_m \tag{22a}$$

$$X_m^{k+1} = [X_m^k + \Lambda^k(P_t^m - P_{max}^m)]^+, m \in \mathcal{B}_m \tag{22b}$$

$$Y_l^{k+1} = [Y_l^k + \Upsilon^k(P_t^l - P_{max}^l)]^+, l \in \mathcal{B}_l \tag{22c}$$

where $\omega, \Lambda, \Upsilon$ are the diminishing step sizes at the k^{th} iteration. The convergence to the optimal solution is guaranteed if a smaller diminishing step size is chosen [32]. **Algorithm 1** provides a summary of the proposed LDD-based resource allocation algorithm.

Algorithm 1 : Joint resource allocation and mode selection

1: Initialize the dual variables $\boldsymbol{\lambda_u}$, $\boldsymbol{X_m}, \boldsymbol{Y_l}$ and generate fading gains, H parameters
2: For subcarrier pair n and AP $\mathcal{B}$, determine the optimal power allocation by using (18), for the given dual variable
3: Update the dual vector $\boldsymbol{\lambda_u}$, $\boldsymbol{X_m}, \boldsymbol{Y_l}$ using sub-gradient method in (22)
4: Repeat steps until the algorithm converges

V. Simulation Results

In this section, we evaluate the proposed approach and present the system performance, where the Matlab simulation parameters are given in Table II. We analyze Case 2 of CDSA, where the CBS provides both the control plane and data plane, while the DBS only provides the data plane. The DBS operates at both unlicensed mmWave band, 26 GHz, and licensed mmWave band, 60 GHz. In the simulation environment, we assume 6 DBSs located within the geographical coverage region of a single CBS with randomly distributed devices within the region of interest. The maximum transmission ranges of the CBS and the DBSs are assumed to be 1 km and 100 m, respectively. A maximum of ten devices are assumed within the coverage area of a DBS. Moreover, the number of devices outside the coverage area of DBSs and distributed within the coverage area of CBS is also assumed to be 10. The links operating at the sub-6 GHz band follow Rayleigh small-scale fading, whereas Nakagami fading is assumed for the links operating at mmWave bands. The total time slot duration is assumed to be 65,535 μs, which is a combination of the alignment time and the data transmission time [15]. The pilot transmission time for beam alignment phase is considered to be 20 μs, where the pilot transmission time is always less than the total time slot duration.

TABLE II: Simulation Parameters

Parameter	Value	Parameter	Value
α_f^{LoS}	2	C_o	10 dB
α_f^{NLoS}	4	$[N_1, N_2, N_3]$	[100, 192, 192]
$\alpha_{\mu W}$	2.7	φ_l	90
$1/y$	141.4 m	φ_u	90
Std(χ^{LoS})	4 dB	θ_l	45^o
Std(χ_{mmW}^{NLoS})	7.2 dB	θ_u	30^o
Std(χ_{mmW}^{LoS})	5.2 dB	N_o	-174 dBm/Hz

For the sake of analysis, we consider average traffic load at the DBS and we divide a whole day into 24 equal time intervals, where each interval has a duration of one hour, i.e., $t \in \{t_1, t_2, \cdots, t_{24}\}$. Self-learning traffic prediction mechanism is employed to predict the average traffic load using the historical call data records. A support vector machine (SVM) regression model is utilized and the historical data is segregated into the training and testing datasets. The training dataset is used in the prediction module to predict the average traffic load for each DBS. The traffic prediction module ascertains the accuracy of the prediction mechanism by utilizing the testing dataset. For the sake of analysis, we assume a constant value of the traffic load between two time intervals. The devices are assumed to be moving randomly with the speed of 3 km/hr. The movement of the devices is assumed to be restricted within the DBSs and CBSs coverage region.

Before proceeding with the EE/SE analysis, we describe two blockage models, ***Blockage Model 1*** **(BM1)** and ***Blockage Model 2*** **(BM2)**, for analyzing the dual-band mmWave DBS. In BM1, the link between the user and the DBS is considered LoS if the user falls within a critical radius R_C around the DBS. The users outside the R_C are considered to be NLoS users [33]. In BM2, the status of the user as a LoS or NLoS is decided on the basis of LoS probability function that depends on the distance between the user and the DBS [29]. Fig. 2a and Fig. 2b present the achievable rates for DBS_1 based on BM1 and DBS_2 based on BM2, at different LoS and NLoS path loss exponent α_f^{LoS} and path loss exponent α_f^{NLoS}, respectively. The maximum range of each DBS is 100 m and $R_c = 50m$. It can be seen that BM1 leads to lower achievable rate at

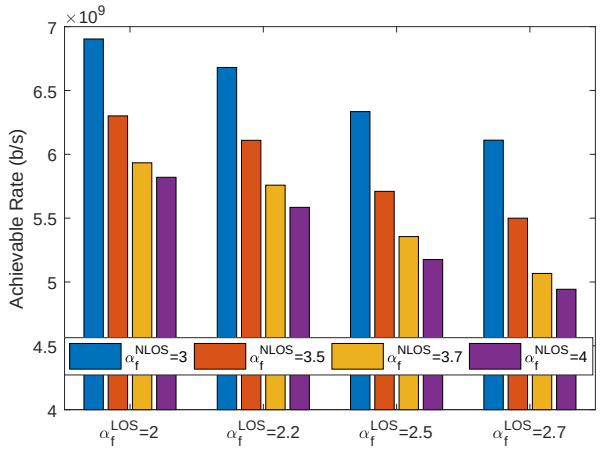

(a) The achievable rate of DBS_1 at Blockage Model 1

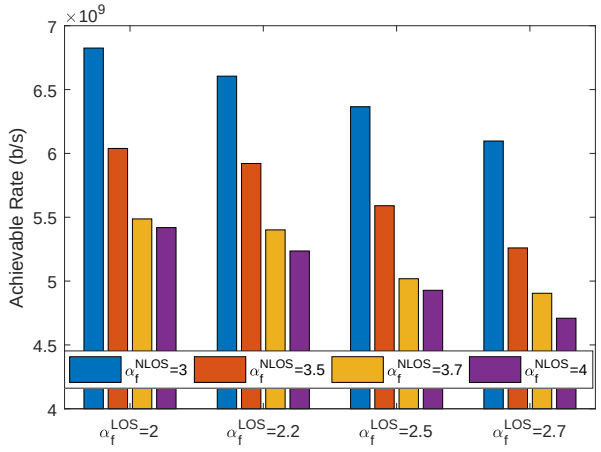

(b) The achievable rate of DBS_2 at Blockage Model 2

Fig. 2: Achievable rate for different LoS and NLoS path loss exponents for DBS_1 and DBS_2.

DBS_1 as compared to BM2 at DBS_2. The main reason for lower achievable rate of BM1 is due to the fact that all the users falling outside R_c are considered to be NLoS, which might not always be true. BM2 uses the probability function to determine if the user is LoS or NLoS, thereby providing a more practical approach towards evaluating the network. We, therefore, evaluate the rest of our results by utilizing BM2.

It is assumed that there are N_1 resource blocks (RBs) exclusively reserved for the CBS operating at f_1 band based on its operating bandwidth, whereas the total number of RBs at DBSs operating at f_2 and f_3 bands are assumed to be N_2 and N_3, respectively. The total number of RBs at the CBS can be divided into two orthogonal sub-partitions, namely as $N_1^{(DBS)}$ and $\tilde{N}_1$. $N_1^{(DBS)}$ is the set of RBs reserved exclusively for the unserved devices covered by the DBSs while initiating the data connections with the CBS. $\tilde{N}_1$ can be further repartitioned into $N_1^{(CBS)}$ and $N_1^{(con)}$, where $N_1^{(CBS)}$ is the set of RBs that serve the devices that are provided data coverage by the CBS, and $N_1^{(con)}$ is the set of RBs reserved for the control and signaling mechanisms of the CBS. For the simplicity of the analysis, we define the proportion of the RBs reserved by the CBS for providing data transmission to the unserved devices lying within the DBS by $\chi = \frac{N_1^{DBS}}{N_1}$. Similarly, the proportion of the RBs reserved by the CBS for providing data transmission to the unserved devices lying within the CBS by $\beta = \frac{N_1^{(CBS)}}{\tilde{N}_1}$.

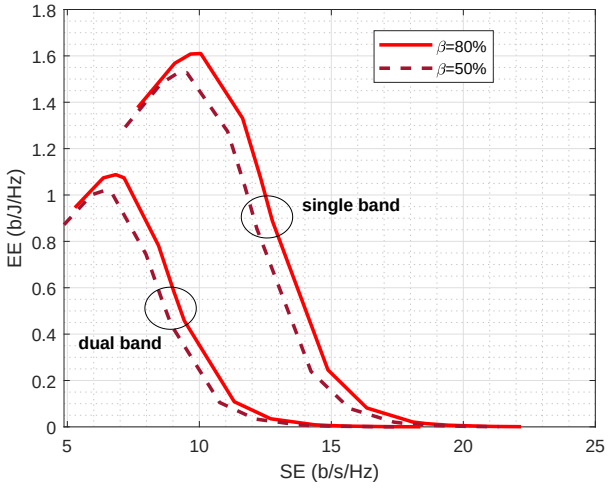

(a) SE versus EE comparison for single-band and dual-band scenarios; χ = 50%

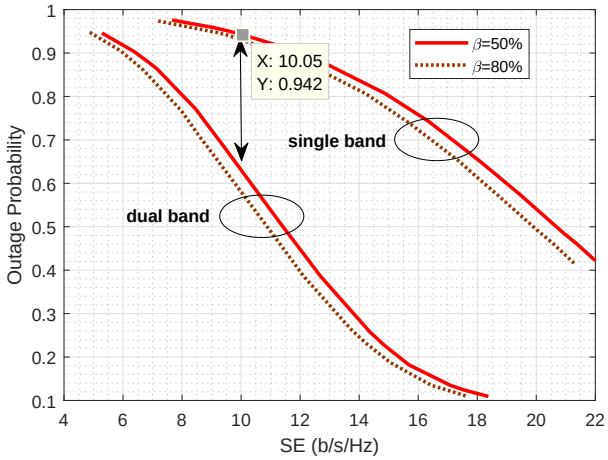

(b) Outage probability comparison between single-band and dual-band scenarios; χ = 50%

Fig. 3: SE versus EE and outage probability comparison between single-band and dual-band scenarios

In Fig. 3a and Fig. 3b, we present the comparison between the single-band and dual-band cases. It can be observed from Fig. 3a that single-band case provides a better performance in terms of EE and SE as compared to the dual-band case for both scenarios of β = 50% and β = 80%. However, Fig. 3b reveals that the single-band case has higher outage probability as compared to the dual-band case. For instance, at the same achievable SE of 10 b/s/Hz, the performance of single band case is 47% worse than dual-band case in terms of outage probability. This highlights the fact that for single band case more users are in outage as compared to the dual-band case, making the dual-band a fair approach as compared to the single band case. It is important to ensure that the users in the network experience a lower outage probability, thereby enhancing network reliability. The outage probability

is defined as the probability of the user's rate falling below a minimum threshold R_{min}, where R_{min} = 0.1 Gbits/s.

Fig. 4 presents the comparison between the proposed LDD-based scheme and the maximal-rate (maxRx), dynamic sub-carrier allocation (DSA) [34] and joint power and rate adaptation (JPRA) [35]. The aforementioned schemes are discussed in the following. The priority of the objectives is dynamically tuned to show the EE-SE tradeoff, which corresponds to the Pareto optimal solution at χ = 50% and several values of β. The results in Fig. 4 are presented for the 5^{th} measuring time interval denoted by t_5. The maximum number of users served by the DBS are assumed to be 10. The traffic prediction module is utilized to predict the average traffic load, i.e., L_{DBS} = [50% 30% 30% 60% 20% 30%] at t_5, where L_{DBS} = 100% signifies that the particular DBS is serving all 10 users at the particular time interval. Similarly, L_{DBS} = 50% denotes 50% loading, i.e., DBS is serving 5 users out of a total of 10.

- **Maximal-rate (maxRx):** In this scheme, the first step is based on assigning all the sub-carriers with equal transmit power. This step is based on the assumption of equal water-filling level for all users. In the next step, the sum rate is maximized by conducting sub-carrier allocation with the BSs. This scheme leads to a single objective problem, where the achievable EE and SE at χ = 50% and several values of β is shown in Fig. 4. If we observe at χ = 50%, β = 50%, MaxRx scheme provides a higher SE but a lower EE as compared to the LDD-based scheme. This behavior is a result of the higher power consumption by MaxRx scheme. However, if we observe at β = [60% 70% 80%], MaxRx scheme provides lower SE and EE as compared to LDD-based scheme.
- **Dynamic sub-carrier allocation (DSA):** In the first, the worst sub-carriers are eliminated from the total pool of sub-carriers. Next, the remaining sub-carriers are assigned equal transmit power. The process is reduced to a single objective problem. The sum rate is maximized by conducting the user and sub-carrier allocation. It can be observed from Fig. 4 that the LDD-based scheme provides a higher SE and EE, as compared to the DSA scheme.
- **Joint power and rate adaptation (JPRA):** In the first step of JPRA, the worst sub-carriers are eliminated and the power associated with eliminated sub-carriers is added to the total available power. The total power is then distributed among the remaining sub-carriers. In this scheme, fixed sub-carrier allocation is considered while the power allocation is conducted by employing multi-level water-filling approach. The aim is to maximize the total number of bits transmitted at each sub-carrier. JPRA leads to a lower SE and EE as compared to the LDD-based scheme. In JPRA, the network capacity is adversely affected by the sub-carrier elimination, which leads to a lower SE and EE.

In Fig. 4, if we observe the Pareto frontier curve results for LDD-based scheme, we can see that an increase in the SE results in an increase in the EE. This trend is observed up to

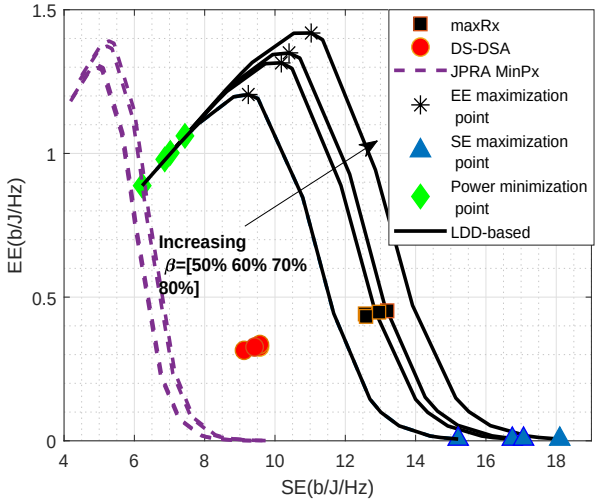

Fig. 4: Energy-efficiency versus spectral-efficiency with χ = 50% and β = [50% 60% 70% 80%] at the measuring time interval t_5, average traffic load L_{DBS} = [50% 30% 30% 60% 20% 30%]

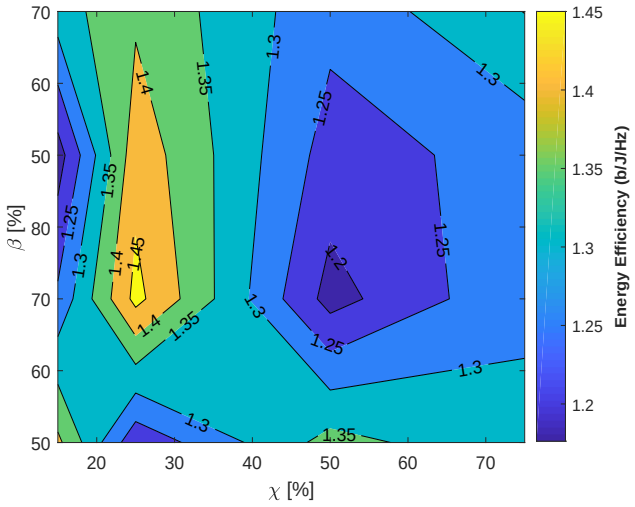

Fig. 5: Energy-efficiency for the different partition sets of (χ,β) at measuring time interval t_1, average traffic load L_{DBS} = [40% 25% 30% 45% 50% 35%]

a peak value due to the dominance of circuit power of the BS as compared to the transmit power. Subsequently, we can observe a sharp decrease in the EE as compared to the SE as the power consumption is dominated by the transmit power, which results in a quasi-concave behavior of EE-SE tradeoff. The sharp decrease in EE after the peak value highlights that a small change in SE has a significant impact on the EE, i.e., a reduction in SE can lead to a sharp increase in the achievable EE. In the figure, we also highlight the power minimization point, the EE maximization point, and the SE maximization point, which are three points of interest with regards to EE-SE tradeoff. Viewing from a network designer's perspective, these points signify the performance regions of the SE-EE tradeoff.

Fig. 5 quantifies the EE versus the different partition sets (χ,β) at time interval t_1. The traffic prediction module provides the average traffic load at t_1, i.e., L_{DBS} =

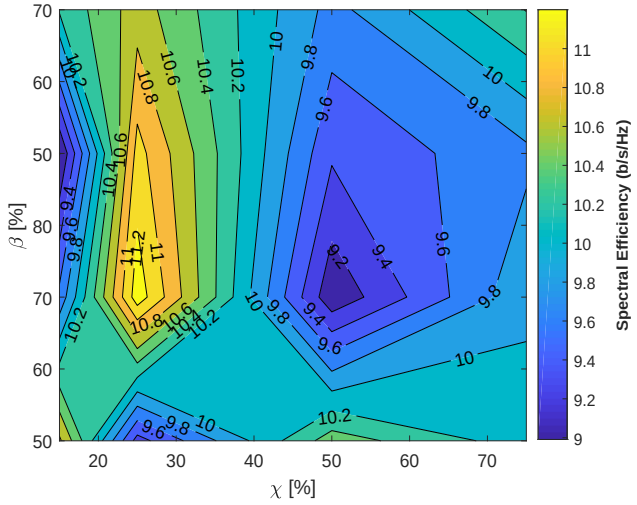

Fig. 6: Spectral-efficiency for the different partition sets of (χ,β) at measuring time interval t_1, L_{DBS} = [40% 30% 20% 50% 60% 30%]

[40% 30% 20% 50% 60% 30%]. It can be observed from the figure that a maximum EE of 1.45 b/J/Hz is achieved for the partition set (25%, 60%). The EE is also quantified for different partition sets, higlighting the impact of partition sets on the achievable EE. In the similar manner, Fig. 6 presents the SE versus the different partition sets of (χ,β) at t_1. For the partition set (25%, 60%), the achievable SE approximately equals to 11.2 b/s/Hz. It is pertinent to mention that the SE=11.2 b/s/Hz is not the maximum achievable SE. It is the achievable SE for the particular partition set that provides the maximum EE, i.e., 1.45 b/J/Hz at the partition set (25%, 60%). Fig. 5 and Fig. 6 can be used to determine the optimal partition set (χ,β) for achieving the maximum EE and finding the corresponding SE for that partition set. Note that the change in the number of users and the available bandwidth at the CBS can lead to a change in the optimal partition set.

For the proceeding results, we make a distinction between the type of users based on the rate requirements. Let U_{low} denote the percentage of users in the coverage area of DBS that have a low data rate requirement, i.e., users requiring rate less than 0.1 Gb/s. We consider 100% traffic load at the DBS, i.e., each DBS has 10 active users. Fig. 7a and 7b shows the EE that can be achieved for different values of U_{low} and β, for a fixed χ = 50%. It can be observed that the decrease in the number of low data rate users leads to a decrease in the EE and SE. This behavior is observed due to the fact that the number of high data rate users increases as U_{low} decreases. From a designer's perspective, these results are significant in identifying the EE and SE that can be achieved for a particular network setting.

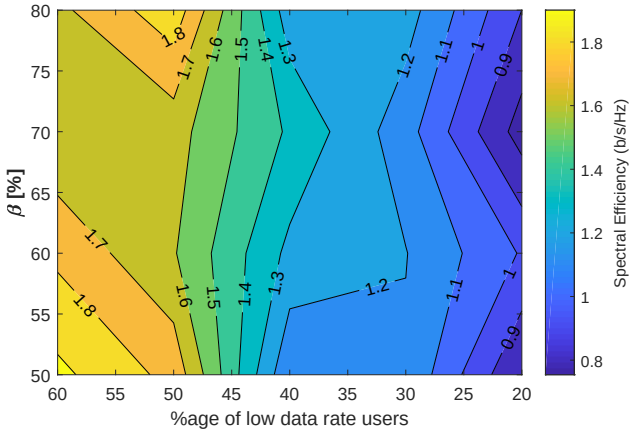

(a) U_{low} versus SE

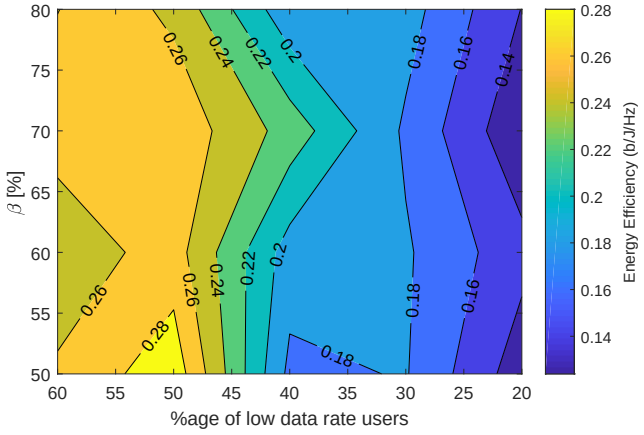

(b) U_{low} versus EE

Fig. 7: SE and EE for different low data rate users.

VI. CONCLUSION

In this article, we motivated a new dimension to spectrum heterogeneity by analyzing a CDSA-based dual-band mmWave network. The DBS possesses a dual-band capability, operating on 26 GHz unlicensed and 60 GHz licensed mmWave band. We presented an overview of the research allocation techniques and discussed the features of CDSA. We also considered the performance metrics that impact the mmWave performance such as antenna characteristics and blockage models. We formulate a multi-objective optimization (MOO) problem to jointly optimize the conflicting objectives: spectral efficiency (SE) and energy efficiency (EE). The unique aspect of this work includes the analysis of a joint radio resource allocation algorithm based on Lagrangian Dual Decomposition (LDD) and we compared the proposed algorithm with the maximal-rate (maxRx), Dynamic sub-carrier allocation (DSA) and Joint power and rate adaptation (JPRA) techniques. The results indicated that the LDD-based algorithm outperforms the aforementioned algorithms in terms of SE and EE. Moreover, we presented a EE-SE tradeoff analysis for the proposed LDD-based scheme by dynamically tuning the priority of both the objectives resulting in the corresponding Pareto optimal solution. The impact of the partition of spectral resources is quantified in terms of achievable EE and SE.

ACKNOWLEDGEMENT

This research work was supported in part by the Erasmus Mundus Action 2 - Strand 1 'LEADERS' project, Grant

Agreement No. 2014 – 0855, funded by the European Union. This work was supported in part through ESPRC UK Global Challenges Research Fund (GCRF) allocation under grant number EP/P028764/1. This work was supported by grant 20150367 from the Swedish Knowledge Foundation.

APPENDIX

PROOF OF PROPOSITION 1

The function C_{u_m} is a concave function of $P_{\mathcal{B},u,n}$, due to the concavity of the logarithmic function. The function $-P_{total}$ depends linearly on $P_{\mathcal{B},u,n}$, making it a concave function. The function given in (14) can be regarded as a weighted Tchebycheff summation of two concave functions.

PROOF OF LEMMA 1

The Karush-Kuhn-Tucker (KKT) condition is applied to the Lagrangian function. The derivative of $\mathcal{L}(\boldsymbol{\rho}, \boldsymbol{p}, \boldsymbol{\lambda_u}, \boldsymbol{X_m}, \boldsymbol{Y_l})$ with respect to $\boldsymbol{p}$ is set to zero to find the optimal power allocation.

$$\frac{\partial \mathcal{L}}{P_{m,u,n}} = 0, and \frac{\partial \mathcal{L}}{P_{l,u,n}} = 0 \tag{23}$$

The application of KKT condition is based on a similar process, so we demonstrate the derivation for the CBS direct mode case only. Constraint C4 ensures that the power is positive.

$$\begin{aligned}
&\Rightarrow \frac{\partial \mathcal{L}}{P^{(d)}_{l,u,n}} = \left(\frac{\Phi}{R_{norm}} + \lambda_u\right)\left(1 - \frac{\tau_{u,l}}{T}\right) \times \\
&w_u \frac{H_2^n}{(1 + P^{(d)}_{l,u,n} H_2^n) ln(2)} - \left(\frac{(1-\Phi)\eta}{P_{norm}} + Y_l\right) = 0 \\
&\Rightarrow \left(\frac{\Phi}{R_{norm}} + \lambda_u\right)\left(1 - \frac{\tau_{u,l}}{T}\right) \frac{w_u}{ln(2)} H_2^{n,n'} = \\
&\left(\frac{(1-\Phi)\eta}{P_{norm}} + Y_l\right)(1 + P_{l,u,n} H_2^n) \\
&\Rightarrow \frac{\left(\frac{\Phi + \lambda_u R_{norm}}{R_{norm}}\right)\left(1 - \frac{\tau_{u,l}}{T}\right)\frac{w_u}{ln(2)} H_2^n}{\left(\frac{(1-\Phi)\eta + Y_l P_{norm}}{P_{norm}}\right)} = \\
&(1 + P^{(d)}_{l,u,(n)} H_2^{n,n'}) \\
&\Rightarrow P_{l,u,(n,n')} = \frac{(1 - \frac{\tau_{u,l}}{T_t}) w_u (\Phi + \lambda_u R_{norm}) P_{norm}}{(Y_l P_{norm} + (1-\Phi)\eta)(ln(2) R_{norm})} - \frac{1}{H_2^{n,n'}}
\end{aligned} \tag{24}$$

REFERENCES

[1] "Cisco visual networking index: Global mobile data traffic forecast update, 2016-2021," Mar 2017. [Online]. Available: www.cisco.com

[2] Z. Yan, W. Zhou, S. Chen, and H. Liu, "Modeling and analysis of two-tier HetNets with cognitive small cells," *IEEE Access*, vol. 5, pp. 2904–2912, 2017.

[3] M. Rebato, F. Boccardi, M. Mezzavilla, S. Rangan, and M. Zorzi, "Hybrid spectrum sharing in mmWave cellular networks," *IEEE Transactions on Cognitive Communications and Networking*, vol. 3, no. 2, pp. 155–168, June 2017.

[4] H. Shokri-Ghadikolaei, F. Boccardi, C. Fischione, G. Fodor, and M. Zorzi, "Spectrum sharing in mmWave cellular networks via cell association, coordination, and beamforming," *IEEE Journal on Selected Areas in Communications*, vol. 34, no. 11, pp. 2902–2917, Nov 2016.

[5] A. Mohamed, O. Onireti, M. A. Imran, A. Imran, and R. Tafazolli, "Control-data separation architecture for cellular radio access networks: A survey and outlook," *IEEE Communications Surveys Tutorials*, vol. 18, no. 1, pp. 446–465, Firstquarter 2016.

[6] H. Munir, S. A. Hassan, H. Pervaiz, Q. Ni, and L. Musavian, "Energy efficient resource allocation in 5G hybrid heterogeneous networks: A game theoretic approach," in *IEEE 84th Vehicular Technology Conference (VTC-Fall)*, Sep. 2016, pp. 1–5.

[7] K. Shen, Y.-F. Liu, D. Y. Ding, and W. Yu, "Flexible multiple base station association and activation for downlink heterogeneous networks," *IEEE Signal Processing Letters*, vol. 24, no. 10, pp. 1498–1502, 2017.

[8] X. Lin and S. Wang, "Joint user association and base station switching on/off for green heterogeneous cellular networks," in *IEEE International Conference on Communications (ICC)*, May 2017, pp. 1–6.

[9] M. S. Omar, S. A. Hassan, H. Pervaiz, Q. Ni, L. Musavian, S. Mumtaz, and O. A. Dobre, "Multiobjective optimization in 5G hybrid networks," *IEEE Internet of Things Journal*, vol. 5, no. 3, pp. 1588–1597, June 2018.

[10] S. Niknam, A. A. Nasir, H. Mehrpouyan, and B. Natarajan, "A multi-band OFDMA heterogeneous network for millimeter wave 5G wireless applications," *IEEE Access*, vol. 4, pp. 5640–5648, 2016.

[11] H. Zhang, S. Huang, C. Jiang, K. Long, V. C. M. Leung, and H. V. Poor, "Energy efficient user association and power allocation in millimeter-wave-based ultra dense networks with energy harvesting base stations," *IEEE Journal on Selected Areas in Communications*, vol. 35, no. 9, pp. 1936–1947, Sept 2017.

[12] P. Trakas, F. Adelantado, N. Zorba, and C. Verikoukis, "A quality of experience-aware association algorithm for 5g heterogeneous networks," in *IEEE International Conference on Communications (ICC)*, May 2017, pp. 1–6.

[13] Q. Ren, J. Fan, X. Luo, Z. Xu, and Y. Chen, "Energy efficient base station deployment scheme in heterogeneous cellular network," in *IEEE 81st Vehicular Technology Conference (VTC Spring)*, May 2015, pp. 1–5.

[14] X. Chai, Y. Li, Y. Lv, and Z. Zhang, "Joint spectrum-sharing and base-station-sleep model for improving energy efficiency of hetnet," in *IEEE International Conference on Communications (ICC)*, June 2015, pp. 1851–1856.

[15] H. H. Yang, G. Geraci, and T. Q. S. Quek, "MIMO HetNets with wireless backhaul: An energy-efficient design," in *IEEE International Conference on Communications (ICC)*, May 2016, pp. 1–6.

[16] H. Munir, H. Pervaiz, S. A. Hassan, L. Musavian, Q. Ni, M. A. Imran, and R. Tafazolli, "Computationally intelligent techniques for resource management in mmwave small cell networks," *IEEE Wireless Communications*, vol. 25, no. 4, pp. 32–39, AUGUST 2018.

[17] K. M. S. Huq, S. Mumtaz, J. Bachmatiuk, J. Rodriguez, X. Wang, and R. L. Aguiar, "Green HetNet CoMP: Energy efficiency analysis and optimization," *IEEE Transactions on Vehicular Technology*, vol. 64, no. 10, pp. 4670–4683, Oct 2015.

[18] C. H. Liu, "On the energy efficiency limit of dense heterogeneous cellular networks," in *IEEE Global Communications Conference (GLOBECOM)*, Dec 2016, pp. 1–7.

[19] C. H. Liu and K. L. Fong, "Fundamentals of the downlink green coverage and energy efficiency in heterogeneous networks," *IEEE Journal on Selected Areas in Communications*, vol. 34, no. 12, pp. 3271–3287, Dec 2016.

[20] H. Pervaiz, L. Musavian, Q. Ni, and Z. Ding, "Energy and spectrum efficient transmission techniques under QoS constraints toward green heterogeneous networks," *IEEE Access*, vol. 3, pp. 1655–1671, 2015.

[21] J. Wang, X. Chu, M. Ding, and D. Lopez-Perez, "On the performance of multi-tier heterogeneous networks under LoS and NLoS transmissions," in *IEEE Globecom Workshops (GC Wkshps)*, Dec 2016, pp. 1–6.

[22] H. Mehrpouyan, M. Matthaiou, R. Wang, G. K. Karagiannidis, and Y. Hua, "Hybrid millimeter-wave systems: a novel paradigm for Hetnets," *IEEE Communications Magazine*, vol. 53, no. 1, pp. 216–221, January 2015.

[23] S. K. Goudos, A. Tsiflikiotis, D. Babas, K. Siakavara, C. Kalialakis, and G. K. Karagiannidis, "Evolutionary design of a dual band e-shaped patch antenna for 5G mobile communications," in *6th International Conference on Modern Circuits and Systems Technologies (MOCAST)*, May 2017, pp. 1–4.

[24] R. O. Adeogun and O. E. Falowo, "Performance analysis of two-tier multiantenna 5G heterogeneous wireless networks with dual band transmission," in *24th International Conference on Telecommunications (ICT)*, May 2017, pp. 1–6.

[25] S. Habib, S. A. Hassan, A. A. Nasir, and H. Mehrpouyan, "Millimeter wave cell search for initial access: Analysis, design, and implemen-

tation," in *13th International Wireless Communications and Mobile Computing Conference (IWCMC)*, June 2017, pp. 922–927.

[26] H. Shokri-Ghadikolaei, L. Gkatzikis, and C. Fischione, "Beam-searching and transmission scheduling in millimeter wave communications," in *IEEE International Conference on Communications (ICC)*, June 2015, pp. 1292–1297.

[27] Y. Li, J. G. Andrews, F. Baccelli, T. D. Novlan, and C. J. Zhang, "Design and analysis of initial access in millimeter wave cellular networks," *IEEE Transactions on Wireless Communications*, vol. 16, no. 10, pp. 6409–6425, Oct 2017.

[28] J. Ryan, G. R. MacCartney, and T. S. Rappaport, "Indoor office wideband penetration loss measurements at 73 GHz," in *IEEE International Conference on Communications Workshops (ICC Workshops)*, May 2017, pp. 228–233.

[29] T. Bai and R. W. Heath, "Coverage and rate analysis for millimeter-wave cellular networks," *IEEE Transactions on Wireless Communications*, vol. 14, no. 2, pp. 1100–1114, Feb 2015.

[30] A. Mahmood, M. M. A. Hossain, and M. Gidlund, "Cross-layer optimization of wireless links under reliability and energy constraints," in *IEEE Wireless Communications and Networking Conference (WCNC)*, April 2018, pp. 1–6.

[31] Z. Song, Q. Ni, K. Navaie, S. Hou, S. Wu, and X. Sun, "On the spectral-energy efficiency and rate fairness tradeoff in relay-aided cooperative ofdma systems," *IEEE Transactions on Wireless Communications*, vol. 15, no. 9, pp. 6342–6355, Sept 2016.

[32] S. Boyd and A. Mutapcic, "Subgradient methods," *Lecture notes of EE364b, Stanford University, Winter Quarter*, 2006.

[33] E. Turgut and M. C. Gursoy, "Coverage in heterogeneous downlink millimeter wave cellular networks," *IEEE Transactions on Communications*, vol. 65, no. 10, pp. 4463–4477, Oct 2017.

[34] D. S. W. Hui, V. K. N. Lau, and W. H. Lam, "Cross-layer design for ofdma wireless systems with heterogeneous delay requirements," *IEEE Transactions on Wireless Communications*, vol. 6, no. 8, pp. 2872–2880, August 2007.

[35] S. Singh, M. Shahbazi, K. Pelechrinis, K. Sundaresan, S. V. Krishnamurthy, and S. Addepalli, "Adaptive sub-carrier level power allocation in OFDMA networks," *IEEE Transactions on Mobile Computing*, vol. 14, no. 1, pp. 28–41, Jan 2015.